Available online at www.sciencedirect.com

SCIENCE DIRECT

Catalysis Today 90 (2004) 93–102

CATALYSIS TODAY

www.elsevier.com/locate/cattod

Studies of processes occurring during alkoxide derived V–O–W unsupported catalyst formation

M. Najbar [a,*], F. Mizukami [b], P. Kornelak [a], A. Wesełucha-Birczyńska [c], B. Borzęcka-Prokop [a], E. Bielańska [d], A. Białas [a], J. Banaś [a], D. Su [e]

[a] Department of Chemistry, Jagiellonian University, 30 060 Cracow, Ingardena 3, Poland
[b] Laboratory for Membrane Chemistry, National Institute of Advanced Industrial Science and Technology (AIST), AIST-Tohoku, Japan
[c] Regional Laboratory of Physicochemical Analyses and Structural Research, Jagiellonian University, 30 060 Cracow, Ingardena 3, Poland
[d] Institute of Metallurgy and Material Science, PAS, Cracow, Reymonta 25, Poland
[e] Department of Inorganic Chemistry, Fritz Haber Institute of the Max Planck Society, Faradayweg 4-6, D-14195 Berlin, Germany

Available online 24 June 2004

Abstract

The aim of this paper is to investigate the processes occurring during V–O–W unsupported catalyst formation in order to gain the knowledge necessary to design supported catalysts. Sol–gel synthesis of V–W hydroxo-oxide hydrate (W:V = 9:1) from tungsten and vanadyl isopropoxides is described. The hydrate structure is shown to be related to $WO_3 \cdot 0.33H_2O$. The role of vanadium in the formation of this structure is discussed. Hydrate dehydration is shown to result in the formation of V–W hydroxo-oxide isostructural with hexagonal WO_3. Further heating of hydroxy-oxide causes a loss of hydroxy groups accompanied by the formation of V–W oxide bronze isostructural with tetragonal WO_3. Annealing the bronze in an air atmosphere results in the removal of vanadium from the bronze crystallites as a results of its surface segregation. The formation of the surface vanadia-like species on WO_3-related crystallites is found to be a result of vanadium segregation. Increasing the annealing temperature causes recrystallisation of the surface species. The synthesis of a V–W/TiO_2 oxide catalyst via a mixed oxide formation in the presence of titania sols followed, by surface vanadium segregation in an air containing atmosphere, is proposed. The application of the knowledge gained during our investigation of the formation of the unsupported V–O–W catalyst to the discussion of the morphology of the V–O–W/Ti(Sn)O_2 (rutile) catalyst is also demonstrated.

Keywords: Unsupported V–O–W catalyst; Sol–gel synthesis; V–W hydroxo-oxide hydrate; V–W oxide bronze; Vanadia-like surface species

1. Introduction

Sol–gel [1,2] as well as advanced complexing-agent assisted sol–gel [2–4] methods allow one to obtain homogeneous multicomponent oxide systems. These methods seem to be suitable for the formation of mixed transition metal oxides. At the same time, however, mixed oxides of transition metals may undergo cation segregation, which in turn leads to the formation of surface species [5–12] that often show good catalytic performance [9,10,12,13].

Thus it seems that formation of mixed oxides followed by cation segregation should be an efficient method of synthesising oxide catalysts with the controlled structure of surface species.

Vanadia–tungsta catalysts are frequently used for hydrocarbon oxidation [14–16], hydrocarbon ammoxidation [17] and NO_x reduction [18–22].

The possibility of forming V–W oxide bronze by evaporating a solution of ammonium methavanadate and ammonium polytungstate in concentrated oxalic acid and calcinating the dry residue at 748 K has previously been described [5]. Cation segregation in air has been shown to cause the formation of vanadia-related surface species [5]. Such species are known to be active in hydrocarbon oxidation [14–16], hydrocarbon ammoxidation [17] and in selective catalytic reduction (SCR) of NO_x [18,21,22] to dinitrogen. Anatase is commonly used as a support of vanadia–tungsta catalysts [18,21,22]. It may be called a structural support due to its good crystallographic fit to the vanadia-like species as

* Corresponding author. Tel.: +48-12-6336377x2011; fax: +48-12-6340515.
E-mail address: mnajbar@chemia.uj.edu.pl (M. Najbar).

0920-5861/$ – see front matter
doi:10.1016/j.cattod.2004.04.013

well as to the V–W oxide bronze phase. However, in the presence of vanadium ions the temperature of anatase→rutile transformation lowers. The transformation may cause vanadia active-phase detachment. To design a stable catalyst, anatase could be replaced by rutile. Because the conventional method of rutile synthesis via anatase annealing does not yield a preparation with a sufficient specific surface area, an alternative method of synthesising rutile has been proposed [13,23]. A small amount of a tin compound was added to force the system to crystallise in the form of rutile. The highest specific surface area of the support was equal to ca. 80 m^2/g and thus very close to that of anatase commonly used in the vanadia–tungsta catalyst for NO_x SCR [21,22]. It could be lowered by increasing the temperature of the support thermal pretreatment to any demanded value [23]. This support should provide a catalyst with high thermal stability. Because an excess of oxalic acid used in conventional V–O–W catalyst synthesis [14,24] may retard the formation of the epitaxial contact between support and V–W oxide bronze, organometallic precursors' hydrolysis performed in the rutile suspension presence seemed the more promising method for catalyst formation [13]. Tungsten and vanadium isopropoxides with comparable hydrolysis rates [25] were chosen as substrates [13]. The hydrolysis resulted in V–O–W hydrate formation isostructural with $WO_3 \cdot 0.33H_2O$ [26] on Ti, Sn rutile support. The catalyst contained rutile and V–W oxide phases. The XPS results for the freshly prepared catalyst and the catalyst additionally annealed at 733 K in air showed that the annealing simultaneously causes a decrease in N_V/N_W ratio and an increase in the support coverage, $(N_V + N_W)/(N_{Ti} + N_{Sn})$, by forms containing V and W [27]. This can be interpreted only as resulting from predominant tungsten segregation on rutile crystallites, which presumably contain V and W additions. Such an occurrence suggested that vanadia-like species are formed mostly due to vanadium segregation on V–W oxide bronze crystallites. The V–O–W catalyst prepared according to the above method proved to be very active in low-temperature NO reduction by ammonia to dinitrogen [13].

The aim of this paper is to gain insight into the processes that occur during the sol–gel synthesis of a V–O–W unsupported catalyst in order to better understand the formation of the supported catalysts. Such knowledge should help to tailor the design of V–O–W supported catalysts with optimal performance in NO_x SCR and hydrocarbon oxidation or ammoxidation.

The processes that occur are assessed on the basis of the structures of: (i) the V–O–W (W:V = 9:1) hydrate that formed in the course of the sol–gel synthesis from tungsten and vanadyl isopropoxides; (ii) the V–O–W hydroxo-oxide created in the course of hydrate dehydration; (iii) the V–O–W oxide that formed due to hydroxo-oxide dehydroxolation; (iv) the vanadia-like surface species that formed on the surface of V–O–W crystallites due to vanadium segregation; and (v) the W oxide that formed after vanadium segregation.

An effort was made to assess the population of vanadia-like active species on rutile and on V–O–W crystallites in a V–O–W/Ti(Sn)O_2 catalyst earlier used for NO reduction by NH_3.

2. Experimental

2.1. V_2O_5–WO_3 solid solution hydrate synthesis

The synthesis of V–O–W mixed oxide hydrates was performed by hydrolysis of vanadium and tungsten isopropoxides at pH = 1.0. To determine possible vanadium influence on the hydrate structure, the WO_3 hydrate was synthesised from tungsten isopropoxide at the same pH.

A vanadium oxyisopropoxide solution in isopropanol was added to a tungsten hexachloride solution in isopropanol in the proportion V:W=1:9. The bluish-green solution that formed after mixing was stirred at 353 K for 1 h. Water was added to isopropoxides until pH 1.0 was achieved. The obtained white precipitate was heated at 353 K for 24 h. Then, using an evaporator, it was dried, at the same temperature for 1 h, after which the colour changed to greyish-white.

To prepare a tungsta hydrate, tungsten hexachloride was dissolved in isopropanol. The obtained blue solution was heated at 353 K and stirred for 1 h. Water then was added until the 1.0 pH was achieved. Treatment of the precipitate was the same as in the case of V–O–W mixed oxide hydrate. The obtained powder was green.

Syntheses of the Ti, Sn rutile support and of the Ti, Sn rutile supported V–O–W (V:W:[Ti+Sn] = 3:27:70) catalyst have been described elsewhere [13,23].

2.2. Measurements

The V–O–W and WO_3 hydrates were identified by powder X-ray diffraction (XRD) as well as FT Raman spectroscopy.

A Philips Analytical PW 3710 XPERT System with Cu Kα (λ = 0.15418 nm, 940 kV, 30 mA) and a secondary beam monochromator at 0.02° steps at a rate of 2 s per step over the range $10^\circ < 2\Theta < 400^\circ$ was used for XRD measurements.

FT Raman spectra were registered using a Bio-Rad FT Raman spectrometer with a Spectra-Physics diode Nd:YAG laser (1064 nm line).

The evolution of V–O–W hydrate during continuous heating was investigated by thermo-gravimetry (TG) and differential thermal analysis (DTA). The identification of phases formed during isothermal heating at 483, 658, 703, 823 and 923 K for 3 h was performed on the basis of powder XRD patterns as well as FT Raman spectra.

The TG and DTA measurements were conducted on a MAC Science TG/DTA 2000 instrument in dry air, flowing at a rate of 100 $cm^3\,min^{-1}$ at a heating rate of 10 $K\,min^{-1}$; α-alumina was used as the reference for DTA.

Secondary electron (SE) images and element mappings were taken with a Philips Scanning Electron Microscope XL with an EDS LINK-ISIS system.

The HREM image was taken with a Philips CM 200 FEG microscope. The specimens for HREM were prepared by dispersing a small amount of powdered catalyst in methanol and depositing it on a holey carbon film supported on a copper grid.

3. Results and discussion

The XRD patterns of WO_3 (a) and V–W mixed oxide (b) hydrates are shown in Fig. 1. All the reflections in the X-ray diffraction pattern of WO_3 hydrate can be ascribed to tungsta monohydrate [28]. Similarly, the reflections in the X-ray diffraction pattern of the mixed oxide hydrate can be attributed to $WO_3{\cdot}0.33H_2O$ [26].

According to Gerand et al. [26], the structure of $WO_3{\cdot}0.33H_2O$ consists of infinite layers of WO_6 and $WO_5(H_2O)$ octahedra sharing their corners to form six- and three-member rings (Fig. 2). The neighbouring layers are shifted in [1 0 0] direction so that the centres of $WO_5(H_2O)$ octahedra of one layer are placed opposite the centres of the hexagonal rings in the next layer. The tungsta monohydrate structure is composed only of the layers of $WO_5(H_2O)$ octahedra joined by Van der Waals forces (Fig. 3) [28]. The $WO_5(H_2O)$ octahedra in the orthorhombic structure of tungsta monohydrate share corners along the [1 0 0] and [0 1 0] directions. It can therefore be concluded that any special property of vanadyl complexes causes the formation of a hydrate structured with three- and six-member rings. Vanadyl isopropoxide is known to form $3[VO(RO)_3]$ oligomers in isopropanol solutions [29]. The hydrolysis of such trimers will cause three-member oligomer formation with hydroxyl bridges. Oxolation of these oligomers may result in hexagonal ring formation.

Fig. 4 presents Raman spectra of tungsta monohydrate (a) and V–O–W hydrate (b). The bands at 880 and 800, 781 and 687, 284 and 250 cm^{-1} result from the vibrations of M–O–M (M = W or V) bridges: asymmetric stretching, bending and symmetric stretching, respectively [30]. The bands at 980 and 376 cm^{-1} can be ascribed to stretching and bending vibrations of the W=O in tungsta monohydrate, and

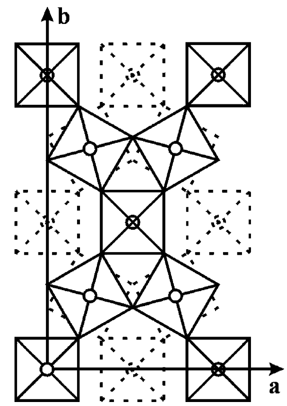

Fig. 2. Projection of $WO_3{\cdot}0.33H_2O$ structure along [0 0 1] direction.

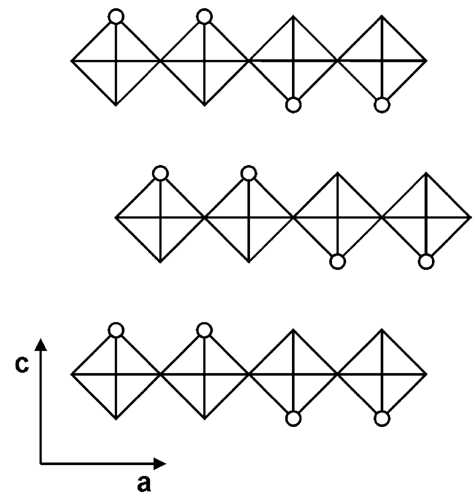

Fig. 3. Projection of $WO_3{\cdot}H_2O$ structure along [0 1 0] direction.

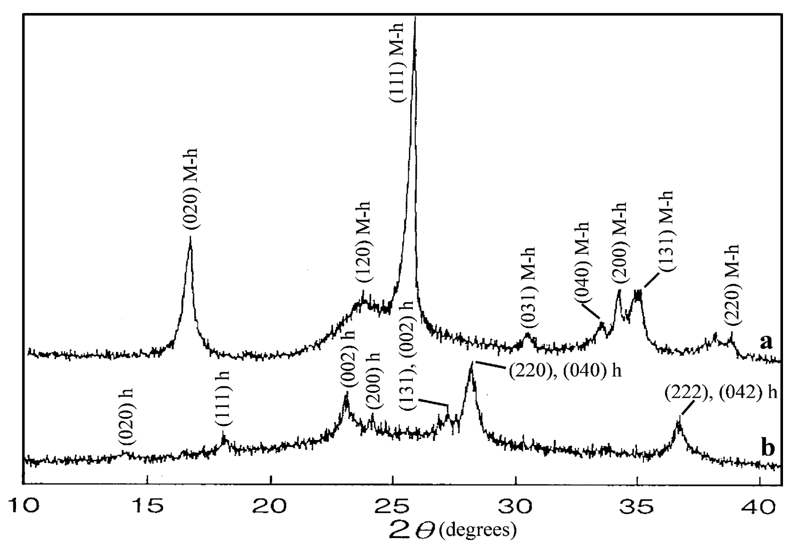

Fig. 1. XRD patterns of the isopropoxy-derived tungsta (a) and isopropoxy-derived V–O–W hydrate (b) (M: h-$WO_3{\cdot}H_2O$, h-$WO_3{\cdot}0.33H_2O$).

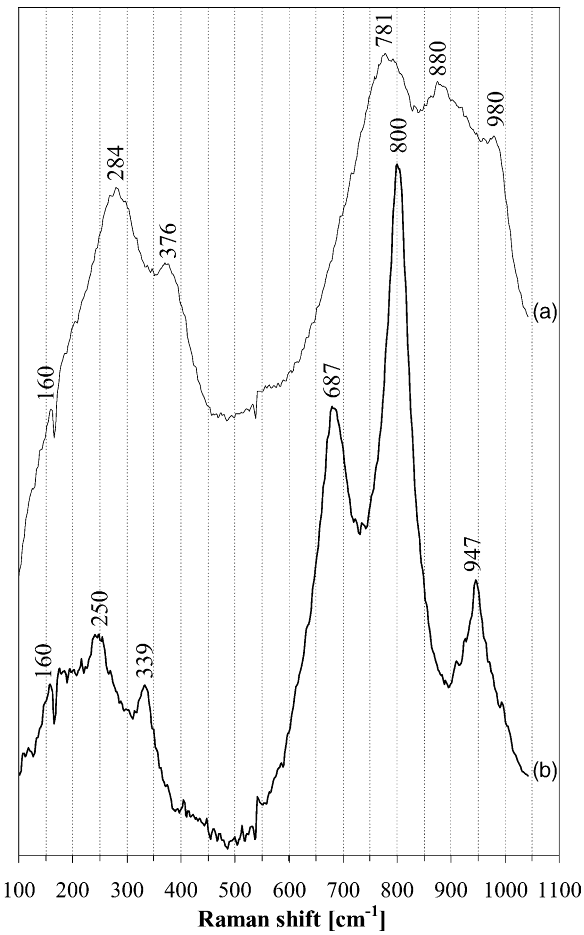

Fig. 4. FT Raman spectra in 100–1040 cm^{-1} range of: $WO_3{\cdot}H_2O$ (a) and V–O–W hydrate (b).

the bands at 947 and 339 cm^{-1} to stretching and bending vibrations of the M=O in the V–O–W hydrate.

Fig. 5 presents the TG (A) and DTA (B) curves for isopropoxo-derived tungsta monohydrate (a) and V–O–W hydrate (b). The TG curve of the tungsta monohydrate clearly shows a two-step weight loss up to 618 K. On the other hand, the TG curve of the V–O–W hydrate demonstrates continuous weight decrease during sample heating up to 703 K, and an additional step weight loss (ca. 0.57%) above this temperature. The dehydration of $WO_3{\cdot}0.33H_2O$ investigated by Gerand et al. [26,31] was found to occur completely during continuous heating up to 673 K. The observed additional weight loss above 703 K can therefore be ascribed to water loss from bridging OH groups that are formed during the hydrolysis of $3[VO(RO)_3]$ oligomers.

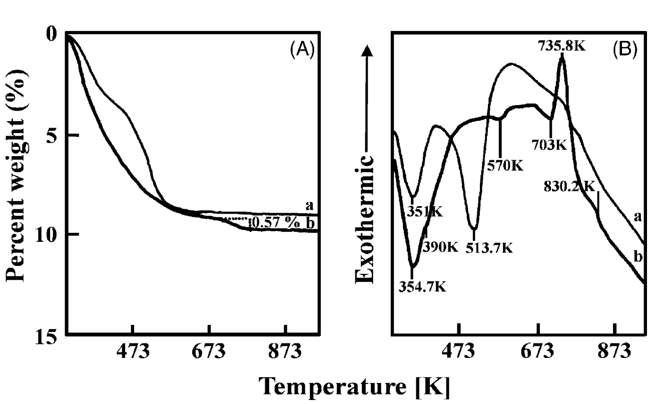

Fig. 5. TG curves (A) and DTA curves (B) for isopropoxy-derived tungsta (a) and isopropoxy-derived V–O–W hydrate (b).

Minima on the DTA curve of tungsta monohydrate may be ascribed, according to Yamaguchi et al. [32], to solvent removal and hydrate dehydration accompanied by cubic tungsta formation. However, the DTA curve of the V–O–W hydrate reveals two endothermic peaks centred at ca. 354.7, 570 K and an endo-exothermic doublet at 703 and 735.8 K, respectively. Two shoulders at ca. 390 and 830.2 K can also be distinguished. The first endothermic peak and the shoulder at ca. 390 K can be ascribed to the loss of volatile compounds (C_3H_7OH, H_2O, and HCl) and hydrate dehydration, respectively. Since the phenomenon presented by the second endothermic peak at 570 K occurs when dehydration is almost completed (curve b in Fig. 5A), it may come from the transformation of dehydrated V–W–O hydrate into the hexagonal phase. Energy is spent in this transformation to shift (0 0 1) layers of half of the identity period in the [1 0 0] direction. According to Figlarz et al. [33], hexagonal WO_3 is stable up to ca. 673 K and transforms at this temperature into the orthorhombic form isostructural with ReO_3, which is composed of straight single chains of WO_6 octahedra connected at their corners. This suggests that the doublet of endo- and exothermic peaks, at 703 and 735.8 K (curve b in Fig. 5B), contains information about processes occurring during hexagonal V–O–W phase transformation into phase built of straight single chains of WO_6 octahedra. The endothermic peak may be an illustration of the energy needed to destroy the hexagonal structure and the endothermic peak of the crystallisation energy of the phase with the structure related to ReO_3. The exothermic peak starts at the same temperature as the step weight loss on the TG curve, which shows that the $3[VO(OH)_3]$ trimers' destruction results in water being released from bridging OH groups. An amount of water (0.57%) is ca. 1.5 times higher than that in $3[VO(OH)_3]$ trimers, therefore allowing one to conclude that some of the tungsten isopropoxides monomers are also involved in the isopropoxide trimers' formation. In light of the above conclusion, it is clear that the composition of the hexagonal phase can be described by the formula $V_{0.1}W_{0.9}(OH)_{0.15}O_{2.875}$. Thus it can be claimed that the sol–gel process in vanadyl and tungsten isopropoxide mixture at pH ca. 1 results in V–O–W hydroxo-oxide hydrate formation. It has also previously been shown [5] that annealing the mixed vanadyl-tungsten oxalates at temperatures close to that of the exothermic peak (748 K) results in the formation of oxide bronze with vanadium atoms in interstitial positions and a structure related to tetragonal tungsta. One can therefore expect the exothermic peak at 735.8 K to correspond to tetragonal V–O–W bronze crystallisation. It

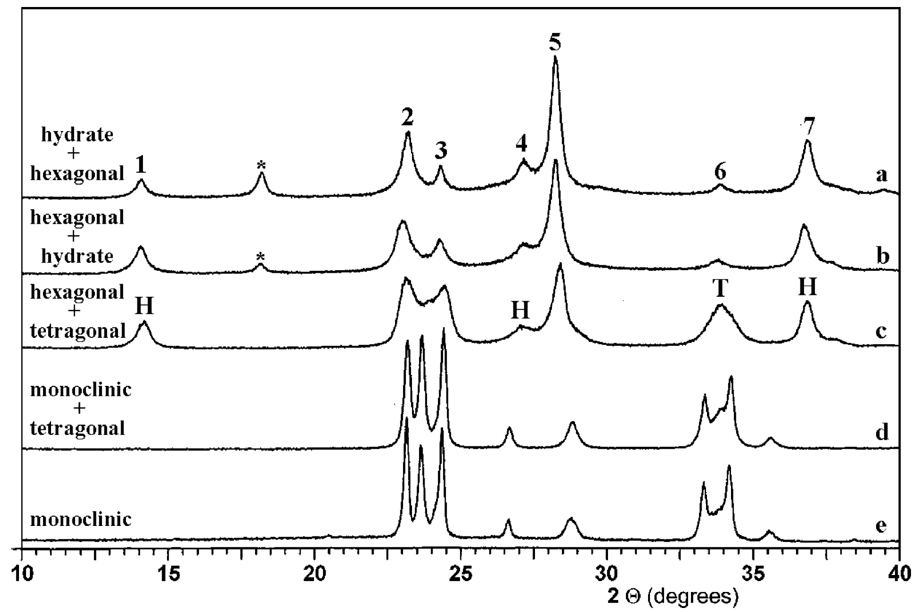

Fig. 6. XRD patterns of the preparations obtained by heating isopropoxy-derived vanadia–tungsta solid solutions at: 483 K (a), 658 K (b), 703 K (c), 823 K (d) and 923 K (e) (1–7 X-ray reflections corresponding to $WO_3{\cdot}0.33H_2O$ [26] as well as to hexagonal WO_3 [31]; ∗: peak corresponding only to $WO_3{\cdot}0.33H_2O$; H: peaks of hexagonal WO_3; T: reflection of tetragonal WO_3 [34]).

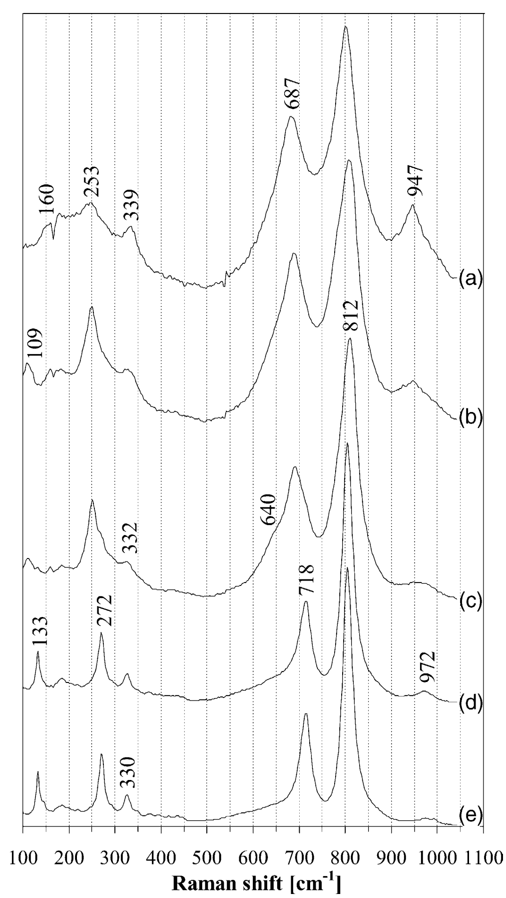

Fig. 7. FT Raman spectra in 100–1040 cm^{-1} range of samples obtained by heating isopropoxy-derived vanadia–tungsta solid solutions at: 483 K (a), 658 K (b), 703 K (c) 823 K (d) and 923 K (e).

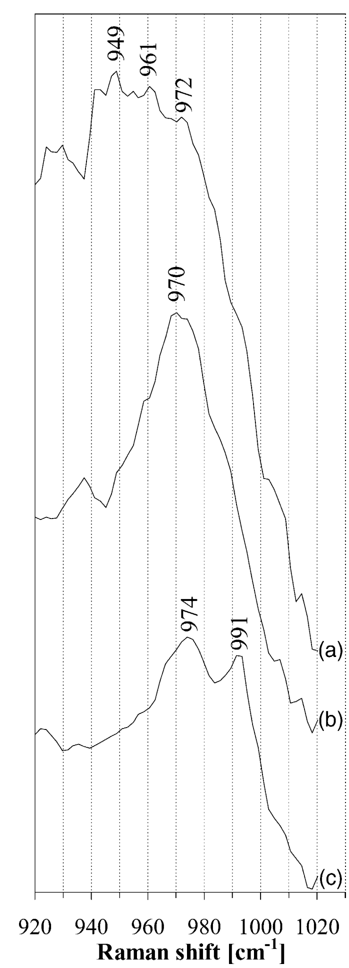

Fig. 8. FT Raman spectra in 920–1020 cm^{-1} range of the preparations obtained by heating isopropoxy-derived vanadia–tungsta solid solutions at: 703 K (a), 823 K (b) and 923 K (c).

has also been found [5] that maintaining the bronze at 813 K in air results in surface vanadium segregation with simultaneous orthorhombic WO_3 formation. This transformation explains the shoulder at ca. 830.2 K.

To verify the assignment of the peaks of the DTA curve (Fig. 5B), XRD patterns and FT Raman spectra were taken for the preparations obtained by V–W–O hydrate annealing consecutively at 483, 658, 703, 823, and 923 K.

The XRD patterns of those preparations are presented in Fig. 6. None of V_2O_5 maxima are observed in the diffraction pattern of the sample annealed at 483 K. All the peaks in this diffraction pattern correspond to $WO_3 \cdot 0.33H_2O$ [26]. The maxima labelled with numbers from 1 to 7 could also be attributed to hexagonal WO_3. To check for the presence of the hexagonal phase, the ratio of the intensity of the (1 1 1) reflection (marked by asterisk) of hydrate to the intensities of the reflections 1–7 were compared with the same ratio for $WO_3 \cdot 0.33H_2O$ [26]. The results are shown in Table 1. The lower values of all the ratios calculated for the investigated sample compared to those for $WO_3 \cdot 0.33H_2O$ show that the sample does contain hexagonal phase beside solid solution hydrate. It can therefore be concluded that partial dehydration accompanied by at least partial transformation of the dehydrated phase into the hexagonal one occurs during isothermal heating at 483 K. A decrease of the relative intensity of the (1 1 1) hydrate reflection due to annealing at 658 K shows further dehydration. The presence of the hydrate in the sample annealed at 658 K suggests that the endothermic peak at 570 K (curve b in Fig. 5B) corresponds to tetragonal → hexagonal transformation occurring only in part of the crystallites (probably the smallest ones). The maxima in the diffraction pattern of the sample annealed at 703 K can be ascribed to hexagonal and tetragonal tungsta phases. The three reflections marked by “H” can be ascribed only to hexagonal WO_3 [31]. One maximum (marked “T”) can predominantly be ascribed to tetragonal WO_3 [34] and the three remaining maxima are composed of those of the tetragonal and hexagonal phases. This shows that tetragonal phase which forms most rapidly at 735.8 K may also be formed at a lower temperature in the course of isothermal annealing. The sample finally annealed at 823 K contains oxide isostructural with monoclinic WO_3 [34] as a major component, and that related to tetragonal tungsta as a minor one. The monoclinic WO_3-related phase was found to be the only component in the preparation finally heated at 923 K. This confirms that the shoulder at 830.2 K (curve b in Fig. 5B) corresponds to the rapid change of tetragonal phase into an orthorhombic one. It should be remembered that in the course of cooling, the orthorhombic phase is transformed into a monoclinic form at 583 K [34]. As shown elsewhere [5], the tetragonal phase changes into an orthorhombic one due to vanadium loss from its structure.

Fig. 7 presents FT Raman spectra of the samples annealed at 483 (a), 658 (b), 703 (c), 823 (d) and 923 K (e), in the 100–1040 cm^{-1} wavenumber range. The lowest value of the M–O–M bending vibration wavenumber, 640 cm^{-1} (Fig. 7c), may easily be explained by the presence of V atoms occupying bronze interstitial positions. Continuous dehydration is demonstrated by the decrease in the intensity of the peak at 947 cm^{-1}. The spectra in the double bond vibration range of the catalysts annealed at 703, 823 and 923 K are presented in Fig. 8. The band at ca. 970 cm^{-1} seen in the spectra of the sample annealed at 703, 823 and

Table 1
Comparison of $(I_{(1\,1\,1)\,\mathrm{hydrate}}/I_{1-7})$ ratio in the sample annealed at 483 K with $(I_{(1\,1\,1)}/I_{1-7})$ in $WO_3 \cdot 0.33H_2O$

Number of (n)	$I_{(1\,1\,1)\,\mathrm{hydrate}}/I_{1-7}$ ratio of the sample annealed at 483 K	hkl	$I_{(1\,1\,1)}/I_{1-7}$ ratio for $WO_3 \cdot 0.33H_2O$ [26]
1	1.331	0 2 0	1.842
2	0.364	0 0 2	0.875
3	0.808	2 0 0	5.000
4	0.706	1 3 1, 0 2 2	1.400
5	0.091	2 2 0, 0 4 0	0.175
6	2.662	2 0 2	5.000
7	0.219	2 2 2, 0 4 2	0.438

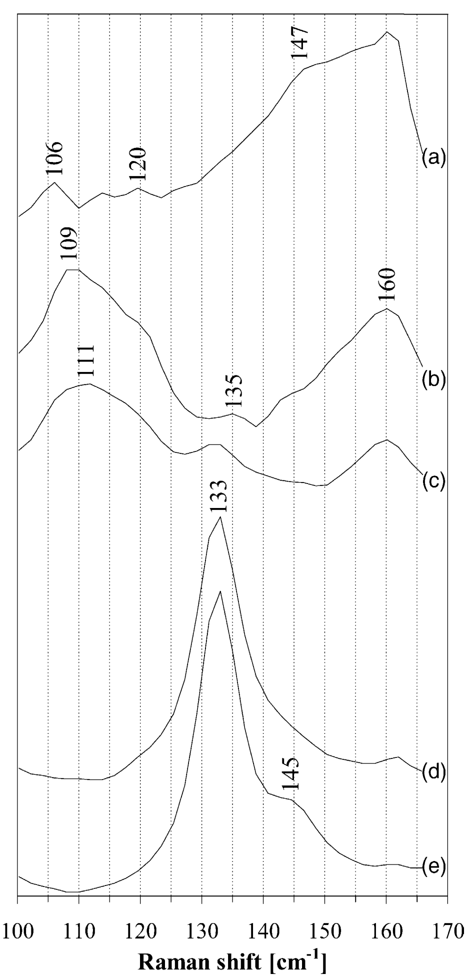

Fig. 9. FT Raman spectra in 100–165 cm^{-1} range of the preparations obtained by heating isopropoxy-derived vanadia–tungsta solid solutions at: 483 K (a), 658 K (b), 703 K (c), 823 K (d) and 923 K (e).

923 K was earlier attributed to a V–O–W layer with vanadia structure on the surface of the V–W oxide bronze crystallites [35]. As those layers are chemically bound with surface bronze layers [35], it is reasonable to conclude that they are vanadia monolayers sharing terminal oxygen with the V–W oxide bronze surface layers. The peak at 961 cm^{-1}, seen in the spectrum of the sample annealed at 703 K, probably comes from vanadyl groups in surface interstitial positions of the V–W oxide bronze crystallites being a precursor of the monolayer. The monolayer species could be formed as a result of vanadyl species migrating on the surface of the crystallites of the V–W oxide bronze. The enlarged spectra in the lattice vibration range are presented in Fig. 9. Comparison of the spectra with X-ray diffraction patterns of the same samples (Fig. 6) and with the DTA curve of V–O–W hydrate (Fig. 5) allowed for the following assignment of the peaks and shoulders:

147 cm^{-1}: V–O–W hydrate isostructural with $WO_3 \cdot 0.33H_2O$;

160 cm^{-1}: V–O–W oxide isostructural with hexagonal WO_3;

106, 109, 111, 120 cm^{-1}: V–W oxide bronzes isostructural with tetragonal WO_3 containing different vanadium amount.

According to published research, the peak at 145 cm^{-1} [36,37] may be attributed to lattice vibrations in V_2O_5 and that at 133 cm^{-1} to monoclinic WO_3 [30]. The presence of a small amount of hexagonal phase at the surface up to 823 K (Fig. 9d) can be explained by the great variety in the crystallite dimensions.

The formation of the crystalline vanadia at the surface of V–W oxide bronze crystallites at 923 K is illustrated by the shoulder at ca. 145 cm^{-1} in lattice vibration range of the Raman spectrum Figs (7e and 9e) and by the peak at ca. 991 cm^{-1} in the double bond vibration range of this spectrum (Fig. 8c). The crystallites are formed at the cost of the monolayer species.

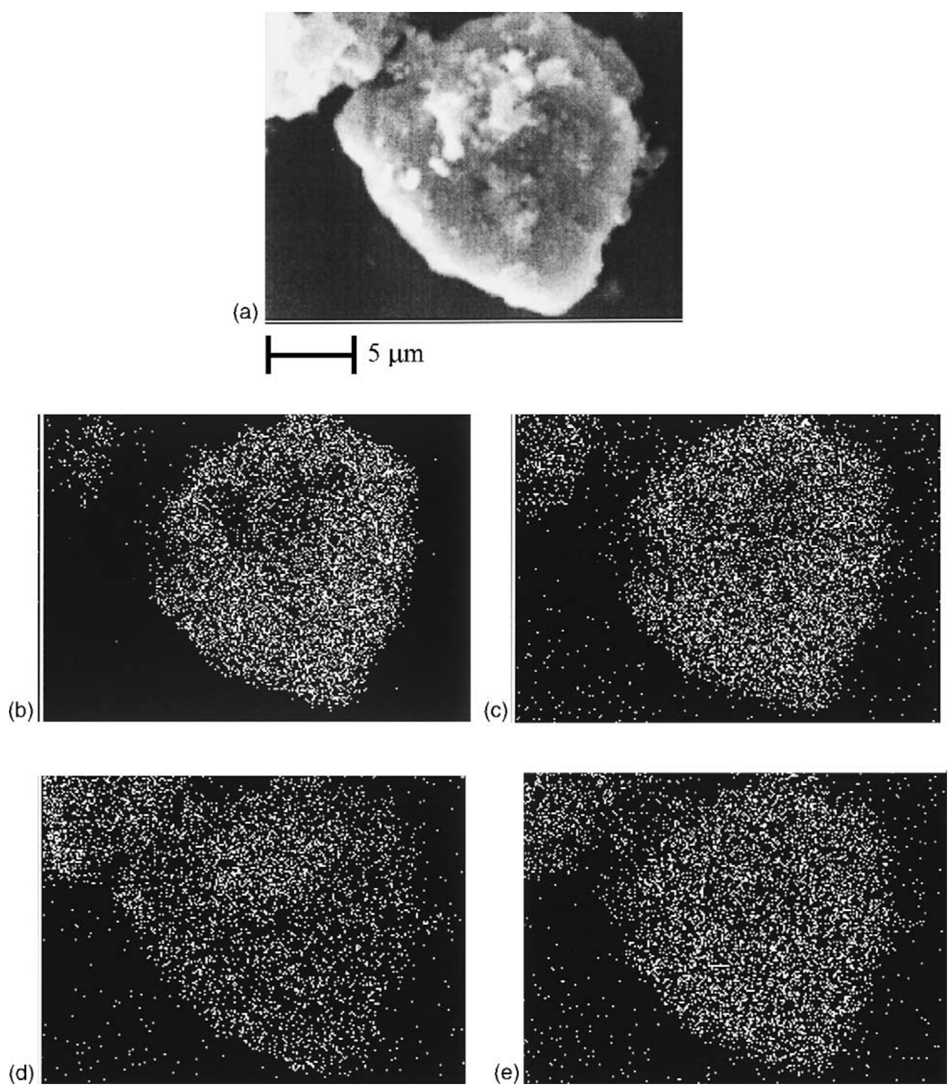

Fig. 10. SE image (a) of particles of the V–O–W/Ti(Sn)O_2 (r) catalyst precursor and element mappings of Ti (b), Sn (c), W (d) and V (e) in microlayers.

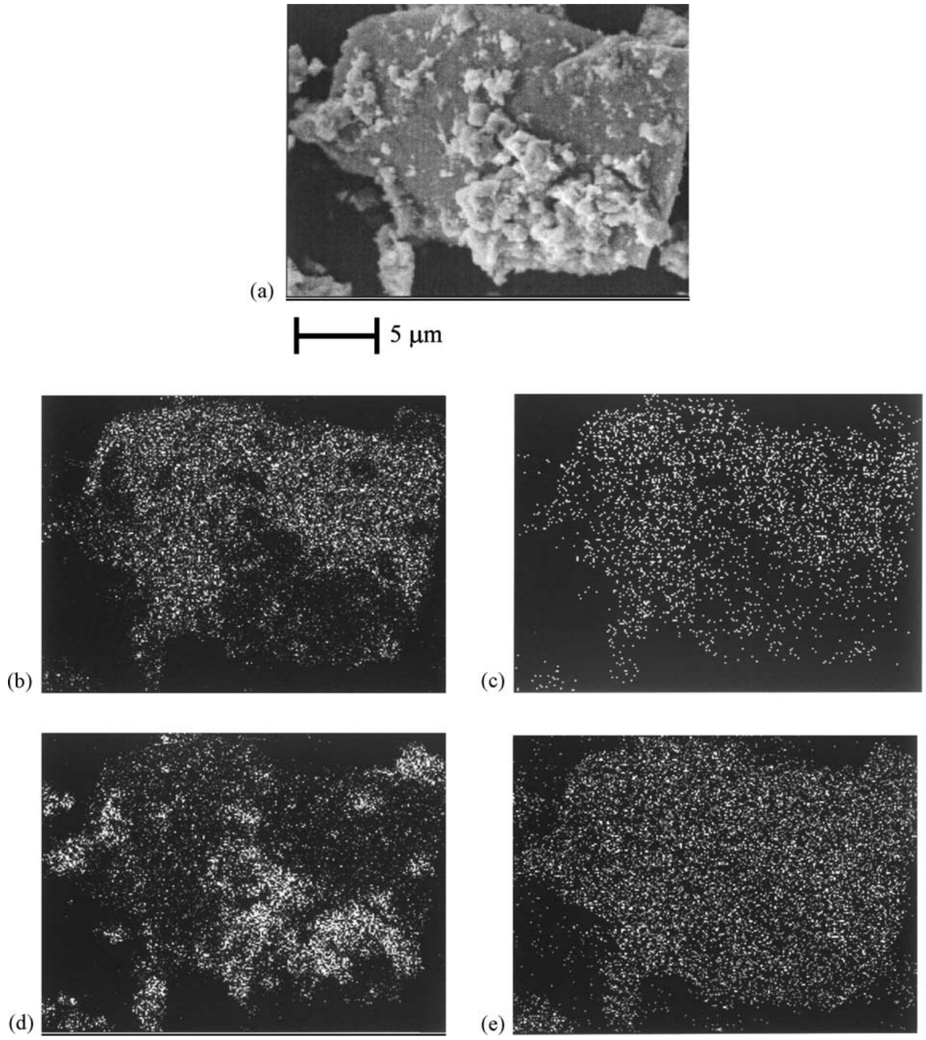

Fig. 11. SE image (a) of particles of the V–O–W/Ti(Sn)O_2 (r) catalyst and element mappings of Ti (b), Sn (c), W (d) and V(e) in microlayers.

Finally applying the knowledge of the processes occurring in the course of unsupported catalyst formation to explain some features of the Ti, Sn rutile supported catalyst is demonstrated. Fig. 10 shows a secondary electron image of particles of the V–O–W/Ti(Sn)O_2 (r) catalyst precursor and element mappings of Ti, Sn, W and V in microlayers. The dimensions of W and V outlines are bigger than those of Ti and Sn. The distribution of particular elements is very similar. Thus an encapsulation of the rutile particles by V–O–W hydrate can be postulated. Fig. 11 presents an SE image as well as Ti, Sn, W and V element mappings of the V–O–W/Ti(Sn)O_2 (r) catalyst. A comparison of the SE images and the element mappings of the catalyst and the precursor shows that migration of the components of V–O–W phase takes place during annealing. As a result encapsulation damage occurs and collecting the V–O–W phase on some areas of the support. Taking into account the results for unsupported V–O–W catalyst presented above, one could conclude that such mobile species are formed during hexagonal → tetragonal phase transformation, after damage of the hexagonal structure and before tetragonal phase crystallisation (see Figs. 5–7). The V element mapping suggests that vanadium is present in the rutile phase as well as in the tungsta-related phase. The results of EDS analysis in microlayers of the areas of Ti, Sn rutile support, Ti, Sn rutile covered by a thin V–W-oxide bronze layer and thick V–W oxide bronze layers, are presented in Table 2. As seen, ca. 6.3 at.% W and 3.8 at.% V dissolve in the analysed Ti, Sn rutile microlayers. The amount of vanadium that dissolves in microlayers of the tungsta-related phase is 1.4 times higher. It can be thus concluded that the catalyst is composed of crystallites of rutile with dissolved W and V atoms and of crystallites of the tungsta-related phase with dissolved vanadium atoms. The dimensions of the crystallites of both phases were determined from HREM images of the catalyst. One such image is shown in Fig. 12, where a few crystallites are visible. Two grains especially stand out, one

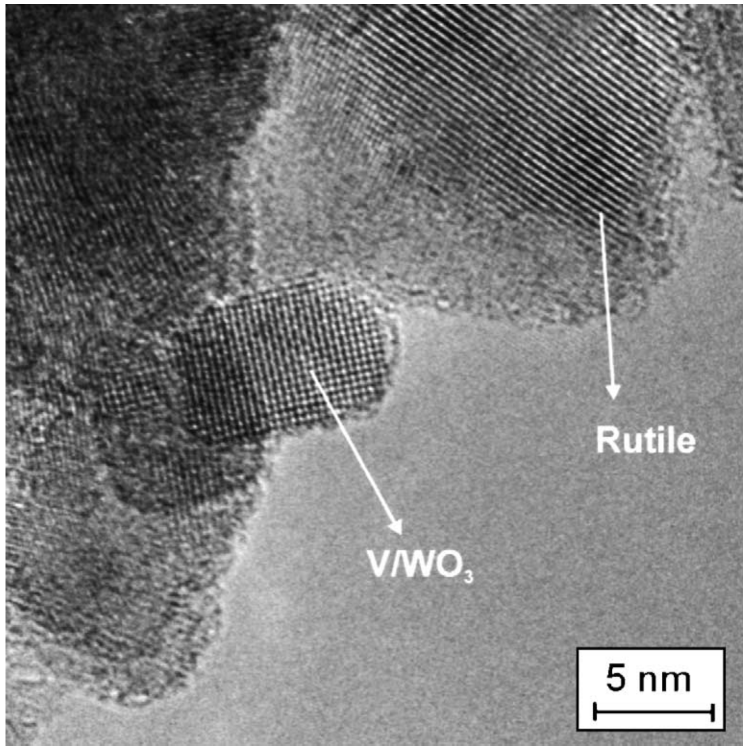

Fig. 12. HRTEM image for the V–O–W/Ti(Sn)O_2 (r) catalyst.

of which has the structure of rutile and the other tetragonal tungsta. The average dimensions determined for tens of rutile crystallites are ca. 9 nm. The average size for the tetragonal V–W oxide bronze crystallites is 8 nm. Thus the procedure yields catalysts with two nanostructured supports. It should be emphasised here that no diminution of the support coverage was observed [27] during annealing of the precursor of the anatase supported V–O–W catalyst. The V–O–W hydrate in that precursor was isostructural with $WO_3 \cdot H_2O$ [38] and therefore V–W oxide bronze formation was not connected with the bonds' breaking. The bronze phase in that catalyst plays the role of an intermediate support.

Table 2
Results of microanalysis performed in areas of V–O–W/Ti(Sn)O_2 (r) catalyst exposing either support or V–O–W bronze phase

Area	Atom (%)			
	V	W	Ti	Sn
Ti, Sn rutile support	3.85	4.29	75.83	16.03
	3.86	5.55	73.04	17.55
	3.86	7.56	72.59	15.99
	3.57	7.03	73.31	16.10
	3.79	6.85	73.32	16.05
Thin V–O–W bronze layer	2.38	9.16	71.01	17.45
on the Ti, Sn rutile support	4.10	14.08	65.01	16.81
Thick V–O–W bronze layer	5.75	49.80	35.29	9.16
on the Ti, Sn rutile support	4.68	53.93	33.78	7.61
	5.94	51.15	34.01	8.91
	5.66	48.90	35.19	10.25

4. Conclusions

The processes occurring during V–O–W isopropoxy-derived unsupported catalyst formation were investigated. Hydrate of V–W hydroxylo-oxide isostructural with $WO_3 \cdot 0.33H_2O$ is formed in the course of sol–gel process at pH ca. 1 from a mixture of vanadyl and tungsten isopropoxides. The hydrate structure was determined by the tendency of the vanadium oxo-isopropoxide to form trimers. V–W hydroxylo-oxide isostructural with hexagonal WO_3 is the primary dehydration product. It is formed by shifting the (0 0 1) layer of the hydrate structure, deprived of water, in the [1 0 0] direction for half the identity period. The collapse of the hexagonal structure, followed by the hydroxyl groups' elimination and crystallisation of V–W oxide bronze isostructural with tetragonal tungsta occurs during further heating of the hexagonal phase. When the tetragonal phase loses enough vanadium due to surface segregation, it transforms into an orthorhombic one. Surface interstitial vanadyl groups appear as the primary surface species. Their migration results in vanadia-like monolayer formation. In the course of further heating, crystalline vanadia-like species are formed. The morphology of Ti, Sn rutile supported catalyst (V:W:Ti:Sn = 3:27:54:16) was discussed using knowledge gained during the investigation of the formation of the unsupported catalyst.

References

[1] F. Mizukami, S. Niwa, M. Toba, T. Tsuchiya, K. Shimizu, S. Imai, J. Imamura, Stud. Surf. Sci. Catal. 31 (1987) 45.
[2] S. Niwa, F. Mizukami, S. Isoyama, T. Tsuchiya, K. Shimizu, S. Imai, J. Imamura, J. Chem. Tech. Biotechnol. 36 (1986) 236.
[3] M. Toba, F. Mizukami, S. Niwa, T. Sano, K. Maeda, A. Annila, V. Komppa, J. Mol. Catal. 91 (1994) 277.
[4] M. Toba, F. Mizukami, S. Niwa, Y. Kiyozumi, K. Maeda, A. Anilla, V. Komppa, J. Mater. Chem. 4 (1994) 585.
[5] M. Najbar, J. Camra, A. Białas, A. Wesełucha-Birczyńska, B. Borzęcka-Prokop, L. Delevoye, J. Klinowski, Phys. Chem. Chem. Phys. 1 (1999) 4645.
[6] M. Najbar, S. Nizioł, J. Solid State Chem. 26 (1978) 339.
[7] A. Bielański, J. Camra, M. Najbar, J. Catal. 57 (1979) 326.
[8] M. Najbar, J. Chem. Soc., Faraday Trans. 82 (1986) 1673.
[9] M. Najbar, A. Białas, J. Camra, B. Borzęcka-Prokop, Proceedings of the I International Symposium on Environmental Catalysis, Piza, 1995, p. 283.
[10] M. Najbar, W. Wal, J. Chrząszcz, Stud. Surf. Sci. Catal. 55 (1990) 779.
[11] M. Najbar, E. Brocławik, A. Góra, J. Camra, A. Białas, A. Wesełucha-Birczyńska, Chem. Phys. Lett. 325 (2000) 330.
[12] A. Bielański, M. Najbar, Appl. Catal. 157 (1997) 223.
[13] M. Najbar, F. Mizukami, A. Białas, J. Camra, A. Wesełucha-Birczyńska, H. Izutsu, A. Góra, Top. Catal. 11/12 (2000) 131.
[14] A. Satsuma, F. Okada, A. Hattori, A. Miyamoto, T. Hattori, Y. Murakami, Appl. Catal. 72 (1991) 295.
[15] T. Ono, Y. Nakanishi, Y. Okuda, Jpn. Kokai 57 (1973) 947.
[16] A. Yasui, T. Minakami, Japanese Patent 10 694 (1972).
[17] US Patent 3 312 710 (1967).
[18] H. Bosch, F. Janssen, Catal. Today 2 (1988) 369.
[19] Japanese Patent 46 463 (1976).
[20] Japanese Patent 97 547 (1981).
[21] P. Forzatti, L. Lietti, HCR Comprehens. Rev. 3 (1996) 33.
[22] G. Busca, L. Lietti, G. Ramis, F. Berti, Appl. Catal. B: Environ. 18 (1998) 1.
[23] A. Białas, E. Bielańska, B. Borzęcka-Prokop, H. Hobert, J. Camra, M. Najbar, J. Sonnefeld, W. Vogelsberger, Pol. J. Environ. Stud. 10 (Suppl. II) (2001) 36.
[24] A. Inglot, M. Najbar, B. Borzęcka-Prokop, J. Chem. Soc., Faraday Trans. 91 (1995) 145.
[25] C.J. Brinker, G. Scherer, Sol–Gel Science, Academic Press Inc., Boston, San Diego, New York, London, Sydney, Tokyo, Toronto, 1990, p. 45.
[26] B. Gerand, G. Nowogrocki, M. Figlarz, J. Solid State Chem. 38 (1981) 312.
[27] M. Najbar, J. Camra, Solid State Ionics 101–103 (1997) 707.
[28] A. Roberts, Geol. Surv. Can. 81-1C (1981) 82.
[29] C.J. Brinker, G. Scherer, Sol–Gel Science, Academic Press Inc., Boston, San Diego, New York, London, Sydney, Tokyo, Toronto, 1990, p. 31.
[30] I. Wachs, F. Hardcastle, S. Chan, Spectroscopy 1 (1986) 30.
[31] B. Gerand, G. Nowogrocki, J. Guenot, M. Figlarz, J. Solid State Chem. 29 (1979) 429.
[32] O. Yamaguchi, D. Tomihisa, H. Kowabata, K. Shimizu, J. Am. Ceram. Soc. 70 (1987) c-94.
[33] M. Figlarz, B. Dumont, B. Gerand, B. Beaudoin, J. Microsc. Electron. 7 (1982) 371.
[34] R. Roth, J. Waring, J. Res. NBS A 70 (1966) 281.
[35] M. Najbar, A. Góra, A. Białas, A. Wesełucha-Birczyńska, Solid State Ionics 141–142 (2001) 499.
[36] T.R. Gilson, O.F. Bizri, N. Cheetham, J. Chem. Soc., Dalton Trans. (1973) 291.
[37] I.R. Beattie, T.R. Gilson, J. Chem. Soc. A (1969) 2322.
[38] M. Najbar, F. Mizukami, H. Izutsu, Pol. J. Environ. Stud. 9 (Suppl. I) (2000) 45.